HHS Public Access

Author manuscript

Matrix Biol. Author manuscript; available in PMC 2018 December 01.

Published in final edited form as:

Matrix Biol. 2018 December ; 74: 101–120. doi:10.1016/j.matbio.2018.07.004.

A scar-like lesion is apparent in basement membrane after wound repair *in vivo*

William Ramos-Lewis,

Department of Cell and Developmental Biology, Program in Developmental Biology, Center for Matrix Biology, Vanderbilt University School of Medicine, Nashville, TN, 37232, USA

Kimberly S. LaFever, and

Department of Cell and Developmental Biology, Program in Developmental Biology, Center for Matrix Biology, Vanderbilt University School of Medicine, Nashville, TN, 37232, USA

Andrea Page-McCaw*

Department of Cell and Developmental Biology, Program in Developmental Biology, Center for Matrix Biology, Vanderbilt University School of Medicine, Nashville, TN, 37232, USA

Abstract

Basement membrane is a highly conserved sheet-like extracellular matrix in animals, underlying simple and complex epithelia, and wrapping around tissues like muscles and nerves. Like the tissues they support, basement membranes become damaged by environmental insults. Although it is clear that basement membranes are repaired after damage, virtually nothing is known about this process. For example, it is not known how repaired basement membranes compare to undamaged ones, whether basement membrane components are necessary for epithelial wound closure, or whether there is a hierarchy of assembly that repairing basement membranes follow, similar to the hierarchy of assembly of embryonic basement membranes. In this report, we address these questions using the basement membrane of the *Drosophila* larval epidermis as a model system. By analyzing the four main basement membrane proteins – laminin, collagen IV, perlecan, and nidogen – we find that although basement membranes are repaired within a day after mechanical damage *in vivo*, thickened and disorganized matrix scars are evident with all four protein components. The new matrix proteins that repair damaged basement membranes are provided by distant adipose and muscle tissues rather than by the local epithelium, the same distant tissues that provide matrix proteins for growth of unwounded basement membranes. To identify a hierarchy of repair, we tested the dependency of each of the basement membrane proteins on the others for incorporation after damage. For proper incorporation after damage, nidogen requires laminin, and perlecan requires collagen IV, but surprisingly collagen IV does not to depend on laminin. Thus, the rules of basement membrane repair are subtly different than those for *de novo* assembly.

*Correspondence andrea.page-mccaw@vanderbilt.edu.

Introduction

Basement membrane is the most ancient and conserved type of extracellular matrix in the animal kingdom [1], and it lies under the basal surface of epithelia and wraps around muscles, nerves, and other organs [2]. Basement membrane is also important for signaling, as it can interact with signaling ligands both to promote their activity [3] and conversely to constrain their diffusion [4]. Experimentally, it has been shown that basement membrane confers mechanical stiffness to tissues, important for shaping organs and determining cellular behaviors [5–9]. Because of such mechanical functions, the dynamic nature of basement membranes has often been overlooked, but these matrix structures expand and shrink along with tissue growth and destruction, and they must be repaired after injury. These dynamic activities occur in the context of continuing basement membrane mechanical functions.

Basement membranes are composed of four main types of glycoproteins and proteoglycans: laminin, collagen IV, nidogen, and perlecan, and these have been analyzed *in vitro* and *in vivo*. The first is laminin, a heterotrimeric protein that polymerizes into a two-dimensional scaffold. Laminin binds directly to cell-surface molecules such as integrins and dystroglycans, and these cell surface interactions increase the local concentration of laminin to promote polymerization at cell membranes [10], which appears to be the first step of making a new basement membrane. The second glycoprotein is collagen IV, a non-fibrillar collagen that assembles into a covalently reinforced sheet that gives basement membrane its mechanical stiffness. Although collagen IV can self-assemble *in vitro* [11], *in vivo* the *de novo* assembly of collagen IV into an embryonic basement membrane requires the presence of laminin in both mice and flies [12,13]. The glycoprotein nidogen binds to laminin and collagen IV *in vitro* [14–16]. Finally, perlecan is a large heparan sulfate proteoglycan [17], which binds with high affinity to nidogen *in vitro* [18]; yet *in vivo*, perlecan requires collagen IV for its deposition into basement membranes of the fly wing disc [19]. Thus, the binding interactions of these matrix proteins *in vitro* and the genetic data from animal studies suggest a partial hierarchy of assembly *in vivo*: laminin, then collagen IV, then perlecan.

In contrast with basement membrane assembly, there is a paucity of information about how the basement membrane is repaired after damage. Repairing basement membrane is important, as epidermal basement membranes become damaged after sun (UV) exposure, possibly contributing to skin aging [20]; damage of the glomerular basement membrane leads to renal disease [21]; and basement membrane repair after corneal injury appears to reverse injury-induced visual haze [22]. The repair of injury-induced basement membrane damage has been studied primarily in the cornea. When the corneal epithelium and adjacent basement membrane were removed in experimentally-induced wounds, epithelial cells closed the wounds within 4–6 days. Around this time, patches of repaired basement membrane were evident, and after 4 weeks increased levels of laminin and collagen IV were detected [23]. However, the repaired basement membrane became functional in terms of cell adhesion only after months [24]. These studies establish that the basement membrane can be repaired after wounding and suggest it may be altered after repair. To date, no studies have manipulated the various basement membrane components to examine the effect on its repair.

We have chosen to analyze basement membrane repair in the fruit fly, *Drosophila melanogaster*. Like vertebrates, *Drosophila* has the same core conserved basement membrane components of laminin, collagen IV, nidogen, and perlecan. An advantage of *Drosophila* over vertebrates, however, is that there are far fewer genes encoding each component, making it easier to eliminate components of basement membranes. For example, targeting *LanB1* knocks down all laminin heterotrimers; targeting either *vkg* or *Col4a1* knocks down all collagen IV heterotrimers; targeting *Ndg* knocks down the single nidogen gene, and targeting *trol* knocks down the single perlecan gene [9]. The sophisticated genetic tools of *Drosophila* further allow for spatial and temporal knockdown of each gene. Finally, each of these core basement membrane proteins has been tagged with GFP to permit easy visualization.

In this study, we analyze the repair of the epidermal basement membrane in larvae after a mechanical wound about 100–200 μm across. In similar *Drosophila* larval wounds, it has been observed that basement membrane is present on epidermal cells as they migrate to close the wound [25]. Although this observation seems to suggest that the epidermal cells secrete the repairing basement membrane components, we report here that both unwounded and repaired epidermal basement membrane is assembled from proteins secreted from adipose and muscle tissue. Further, we show that basement membrane is repaired within 24h after damage, although each component repairs with a visible scar. We investigate the requirements for assembly and find that collagen IV is incorporated into these wound sites independently of the synthesis of new laminin, unlike newly assembled embryonic basement membranes. Not every protein incorporates independently, however, because we find that nidogen requires laminin, and perlecan requires collagen IV for proper assembly into the repairing basement membrane.

Results

A lesion in the basement membrane at the site of repair

To analyze basement membrane repair, we utilized an established larval epidermal pinch-wound assay first described by Galko et al [25]. The larval epidermis is an epithelial monolayer of extremely flat cells, roughly 40 μm in diameter and 3 μm thick, with highly polyploid nuclei. On the apical side these cells secrete a thick chitinous cuticle exoskeleton, and on the basal side they sit on a basement membrane, the source of which is not known. To generate epidermal wounds, larvae were pinched with blunted forceps on the dorsal side for approximately 10 seconds to inflict cellular and basement membrane damage without breaking the outer cuticle, resulting in a sterile wound that is not visually occluded by hemolymph clotting (Fig. 1A,B). By 24h after wounding, the wounds had closed. Pinch wounding created a cuticle indentation mirroring the damage to the underlying epithelium, and this indentation remained visible by DIC optics even 24 h after wounding, providing a reliable landmark for the location of the wound during and after repair (Fig. 1B).

To visualize basement membrane proteins, we used a functional GFP-fusion of each of the four main basement membrane proteins (Fig. 1C-F). Collagen IV and perlecan were imaged with *vkg-GFP* and *trol-GFP* protein-traps respectively, in which a GFP exon is inserted into the genomic region, resulting in the GFP fluorescent epitope spliced in-frame into the

endogenous protein. These two GFP-fusion proteins are fully functional, as evidenced by their viability as homozygotes. Functional *LamininB1 (LanB1)-GFP* was provided as a transgene, a recombineered 44 kb genomic fragment encoding a C-terminal fusion of LanB1-GFP that fully rescued a *LanB1* mutant ([26] and our data not shown). *Nidogen (Ndg)-GFP* was also provided as a transgene, a recombineered 36 kb genomic fragment encoding a C-terminal fusion of Nidogen-GFP [26]. When imaged with each of these fusion proteins, the unwounded epidermal basement membrane appeared as a relatively smooth flat surface (Fig. 1C-F), although the epidermal fluorescence from Nidogen-GFP was considerably fainter than the other three fusion proteins. We refer to these four GFP fusion proteins collectively as BM-GFP.

After pinch-wounding, basement membrane and the overlying cells were visibly damaged at the site of the wound (Fig. 1G-J and Fig. S1), and the dimensions of damage were similar for both. Within 24 hours after injury, the basement membrane repaired to a continuous sheet in control animals. Strikingly, the basement membrane formed a lesion at the site of repair, evident with all four BM-GFP proteins (Fig. 1K-N). This lesion was characterized by regions of increased fluorescence, fibril-like in appearance, within the site of repair. These fibril-like structures were thicker than the unwounded basement membrane and were largely excluded from areas occupied by cell nuclei (Fig. 2). Furthermore, the thickening of basement membrane appeared to begin at the wound boundaries within 2 hours after pinch-wounding (Fig. S1). We refer to the matrix lesion that appears after repair as a basement membrane scar. As shown in Figs. 1 and 2, the basement membrane scar is typified by increased abundance of the basement membrane proteins collagen IV, laminin, perlecan, and nidogen in the area where the basement membrane was repaired, resulting in a thicker and more disorganized region of extracellular matrix.

The sources of epithelial basement membrane are the same during normal growth and wound repair.

Since the repaired basement membrane within pinch wounds is morphologically distinct from the surrounding, undamaged basement membrane, the mechanism of repair may also be distinct from normal basement membrane assembly as the animal grows. One way repair might differ from assembly is in the source of each protein. During the 4 days after embryogenesis to the third larval instar, there is a dramatic ~40-fold expansion in epidermal area (8-fold in length and 5-fold in circumference [27]), requiring a similar expansion in basement membrane, but the source of these matrix proteins is not known. One possibility for either the growth source or the wound source is the epidermal cells. However, in *Drosophila*, there are many examples of basement membranes whose component proteins are derived from cellular sources that are not part of the tissue of a given basement membrane [9]. For example, as the *Drosophila* embryo develops, migrating hemocytes deposit matrix proteins to create *de novo* basement membrane throughout the tissues of the embryo, including the epidermis [28,29]. Intriguingly, after larval epidermal wounding, hemocytes are observed at the site of damage [30], so it seemed plausible that they may generate the matrix components required for basement membrane repair. Further, some vertebrate hemocytes secrete perlecan thought to promote wound repair [31]. A third candidate source is adipose tissue: other larval organs, including the wing disc and the

ventral nerve cord, expand their basement membranes during growth by incorporating collagen IV secreted into the hemolymph from the fat body (*Drosophila* adipose tissue that regulates metabolism and immunity [19]). It seemed plausible that epidermal basement membrane might also incorporate collagen IV secreted from the fat body.

To determine the source of basement membrane in unwounded epidermis, we controlled the expression of each of the four BM-GFP fusion proteins in each of these candidate tissues, i.e., epidermis, hemocytes, and fat body, using an RNAi-based strategy. Each candidate tissue was engineered to specifically and constitutively express double-stranded RNA against GFP ($dsRNA^{GFP}$) in flies that contained a single allele of a BM-GFP. Importantly, expression of the wild-type matrix protein continued as normal throughout the animal's life so that the basement membrane itself was never disrupted, eliminating any compensatory mechanisms that might lead to expression from a different source tissue (Fig. 3A). The presence or absence of GFP in the epidermal basement membrane was used to assess the contribution of each candidate tissue (Fig. 3B). To control for the possibility of incomplete knockdown of GFP, we compared the basement membrane fluorescence after candidate tissue knockdowns to the fluorescence after ubiquitous knockdown with *Tub-Gal4* and to the autofluorescence within a tissue (Fig. 3C-F). Since the reliability of these experiments depended on the specificity of each driver used to express $dsRNA^{GFP}$, great care was taken to assess their specificity (Fig. S2), and we confirmed that *c564-Gal4* and *Hml-Gal4* were each specific to fat and hemocytes, respectively. Because the pan-epidermal drivers *A58-Gal4* and *e22C-Gal4* were not specific to epidermis but also expressed in the fat body of 3rd instar larvae (Fig. S2F, G), we knocked down GFP in the epidermis with *pnr-Gal4*, expressed in large patches along the dorsal side of the epidermis. Although the pattern of pnr-Gal4 was not ubiquitous across the epidermis, we did not observe any pattern or patchiness to the epidermal BM fluorescence when each BM-GFP was knocked down with *pnr-Gal4*, nor did we measure any reduction in total fluorescence (Fig. 3).

In unwounded epidermal basement membrane, laminin, collagen IV, and perlecan were found to derive from the fat body. For collagen IV-GFP, expression of $dsRNA^{GFP}$ in the fat body completely eliminated fluorescence from the epidermal basement membrane, with no significant difference between fat-body knockdown and ubiquitous knockdown (Fig. 3D). For laminin-GFP, expression of $dsRNA^{GFP}$ in the fat body eliminated 62% of the fluorescence from the epidermal basement membrane compared to ubiquitous knockdown (Fig. 3C); and for perlecan-GFP, fat-body knockdown eliminated 73% of the fluorescence (Fig. 3E). Thus, although most of the laminin and perlecan in the epidermal basement membrane derive from the fat body, there appears to be a second source that makes a minor contribution. One possibility for this source is leftover laminin-GFP and perlecan-GFP from embryonic epidermal basement membrane deposited by hemocytes, or even from assembled basement membrane around other larval tissues (see Discussion).

To our surprise, nidogen in unwounded epidermal basement membrane did not originate from the fat body, hemocytes, or epidermis. We examined available expression data on nidogen and found that it is highly expressed in muscle progenitors [32]. After confirming the specificity of *Mhc-Gal4* for muscles (Fig. S2D), we tested muscle as a source of each

basement membrane protein in the epidermis; we found that muscle contributes all of the nidogen to the epidermis (Fig. 3F), but does not contribute collagen IV, laminin, or perlecan.

We next asked if the same cellular source that supplied basement membrane proteins to growing epidermis also supplied basement membrane proteins for repair after epidermal wounding. To address this question, we focused on BM-GFP increased fluorescence within the wounded area compared to the background unwounded area: in control animals, the average fluorescence intensity of each of the four BM-GFPs was about two-fold brighter within the wound than outside the wound (Fig. 4). We reasoned that if the source for growth and repair were different, then when we knocked down GFP in the growth source, the repaired basement membrane should retain BM-GFP when the undamaged regions lost GFP, causing an increase in the ratio of fluorescence inside/outside the wound. Conversely, if the source for growth and repair were the same, then when we knocked down GFP in the growth source, significantly less BM-GFP would be incorporated into both the repairing basement membrane and the surrounding unwounded matrix, causing a reduction in fluorescence intensity inside the wound and a constant or decreased ratio inside/outside (see Fig. 4A for a schematic). For all four basement membrane proteins, we found that the ratio of fluorescence intensity decreased when $dsRNA^{GFP}$ knocked down the BM-GFP in the growth source tissue. Thus, our results indicated that basement membrane proteins are secreted from a source tissue and can be incorporated into either expanding basement membrane or damaged basement membrane, with no significant alternative source during wound repair (Fig. 4).

Epidermal cells close wounds in the absence of a fully repaired basement membrane

Next, we sought to test the function of each of the four major basement membrane proteins in wound repair. Because knocking down or mutating laminin, collagen IV, or perlecan is lethal in *Drosophila* [13,33,34], we used the temperature sensitive *Gal4-Gal80^{ts}* system to express dsRNA against each basement membrane component ubiquitously throughout larvae (with *Tub-Gal4*), depleting the animals of newly synthesized basement membrane protein after embryogenesis. Each larva was allowed to grow to 3rd instar, wounded, and allowed to recover for 24h (see Experimental Procedures). Epidermal cells were able to close the wounds when each of the basement membrane proteins was depleted individually (Fig. 5).

In these basement membrane knockdown experiments, larvae knocked down for laminin or collagen IV were observed to be smaller than controls, and those lacking laminin, collagen IV, or perlecan died before adulthood. We expected that as a larva grew, the basement membrane proteins available in the hemolymph at the onset of knockdown would be assembled into extracellular matrices and thus be depleted from the hemolymph. We expected that these two pools could be identified biochemically as a soluble fraction (in the hemolymph) and an insoluble fraction (in the assembled basement membrane). To measure the extent of knockdown, we crossed in one copy of a BM-GFP into the knockdown background and performed anti-GFP western blots on soluble and insoluble larval fractions, as the GFP-tagged protein would be targeted by the same mechanism as the untagged protein. In control larvae, we had limited success in identifying intact basement membrane proteins in the soluble fraction (Fig. S3), although their degradation products could be

readily detected, making it difficult to reproducibly quantify knockdown efficiency in the soluble fractions; but all basement membrane proteins could be reproducibly identified and quantified in the insoluble fraction of larval lysates. In insoluble fractions from whole animals, the average depletion efficiency was about 71% for LanB1, 67% for collagen IV α2 (Viking), 93% for perlecan, and 76% for nidogen, and it appears that the reduction of soluble proteins was even greater (Fig. S3 and Fig. 7C). An important validation of our strategy came from imaging the wounds in the knockdown animals: in every case the knocked-down BM-GFP protein was severely diminished within wound area 24h after wounding, even though the cells had closed the wound (Fig. 6 B,H,N,T). Thus, the knockdown strategy was sufficient to impair basement membrane repair.

Most matrix proteins assemble independently of others during basement membrane repair.

It was previously established that *de novo* basement membrane assembly occurs through a strict hierarchy: laminin creates a foundation that promotes collagen IV assembly, which in turn recruits perlecan [12,13,19]. We sought to determine if this hierarchy of assembly held true during wound repair by analyzing the scar made by each of the four BM-GFP proteins when each basement membrane protein was knocked down. We used the same temporally conditional, spatially ubiquitous strategy of knocking down basement membrane proteins as for examining wound closure, except that we imaged a BM-GFP rather than cells (Fig. 6). Scars in control animals were easily recognizable and consistent, characterized by regions of highly fluorescent BM-GFP staining interspersed with regions of low-intensity fluorescence. We refer to this juxtaposition of high/low fluorescence within the wound as fluorescence anisotropy. To address the requirements for basement membrane assembly in a quantitative manner, we measured the fluorescence anisotropy within the wound boundaries of each sample by measuring the mean fluorescence of the brightest 5% of pixels within the unobstructed wound bed, normalized to the area of low fluorescence within each wound (see Experimental Procedures). Because we found some initial changes in the scars of collagen IV and laminin knockdowns, we tested second dsRNA lines to knock down collagen and laminin, to establish specificity. In agreement with embryo *de novo* assembly data, laminin deposition into the repaired basement membrane did not require any of the other basement membrane proteins (Figure 6A-E, U). Although the intensity of the laminin scar decreased modestly in some samples when collagen IV α2 (*vkg)* was knocked down, this apparent change was not statistically significant ($p \geqq 0.05$) nor was it reproducible when we knocked down collagen IV α1 (*Col4a1*), the obligate partner of collagen IV α2 in the *Drosophila* collagen IV heterotrimer. Depletion of perlecan or nidogen had no effect on laminin anisotropy within the repaired wound (Figure 6U). Therefore, we concluded that laminin deposition into the basement membrane scar was independent from any other basement membrane proteins.

In contrast to what has been reported in embryos, collagen IV deposition into the repaired basement membrane was not perturbed by the depletion of other basement membrane proteins, including the depletion of laminin (Figure 6F-J, V), a surprising result that we tested further (see next section). Next, we analyzed perlecan deposition into the repaired basement membrane and found that it was significantly altered by the depletion of collagen IV (Figure 6K-O, W). Although the accumulation of perlecan in the repaired basement

membrane did not require collagen IV like it does in the growing wing disc [19], when either collagen IVα2 or collagen IVα1 were depleted, perlecan deposition was more uniform within the repaired region of basement membrane (Fig. 6M and Fig. S4D), appearing significantly different from the anisotropy of perlecan in control wounds (Fig. 6W). Finally, for nidogen, measurements of fluorescence anisotropy within the wound showed a significant difference only in the case of laminin depletion (Fig. 6P-T, X). These results were reproduced with two different dsRNA constructs targeting the laminin gene. When laminin was knocked down, nidogen-GFP fluorescence decreased outside the wound area as well as in the scar, indicating that laminin is required for nidogen recruitment to the basement membrane during assembly and/or growth, as well as repair. Thus, in repairing basement membranes, laminin and collagen IV assemble independently of the other protein components, whereas nidogen depends on laminin and perlecan is organized by collagen IV.

Whenever either subunit of collagen IV was knocked down, the basement membrane was noticeably more fragile upon dissection, consistent with the role of collagen IV in determining the mechanical strength of basement membrane. In these knockdowns, the appearance of all the basement membrane proteins was visibly altered both inside and outside the wound, as though the entire basement membrane was scarred even outside the intended wound area, which we find a plausible outcome when collagen IV is not present for support. Because of this extensive change outside the wound, the scar within the wound appeared to spread across the wound bed rather than be focused in the center as in controls (see Figs. 6 and S4). This apparent increase in scarring is evident with all the basement membrane proteins in collagen IV knockdowns.

Collagen IV assembles into basement membrane scars by a different mechanism than *de novo* assembly.

The finding that collagen IV did not require laminin to assemble in wounds suggested two possibilities: 1) collagen IV assembly into basement-membrane scars occurs via a distinct mechanism from that of *de novo* assembly, or 2) the laminin depletion was not efficient enough to observe a phenotype. We reasoned that if the *de novo* and repair mechanisms are the same, and collagen IV requires only a limited amount of laminin to assemble, then a similar efficiency of knockdown would be enough to prevent collagen IV deposition into the basement membrane during *de novo* assembly in embryos. Using the same *LanB1-GFP* and *dsRNA* constructs as for larval wounds, we assessed the efficiency of laminin knockdown in embryos by measuring the fluorescence of Laminin-GFP in stage 16–17 embryos. Fluorescence levels in *LanB1* knockdown embryos were 32% that of controls (Fig. 7A-B). This knockdown efficiency was remarkably similar to what we measured in larvae via western blot, in which Laminin-GFP levels were 29% that of controls (Fig. 7C, Fig. S3). Next we assessed collagen IV assembly in these *LanB1* knockdown embryos, and found that collagen IV-GFP deposition into the basement membrane was disrupted (Fig. 7D) as previously described [12,13], but unlike what we observed for wound repair in larvae. These results indicate that basement membrane repair occurs via a distinct mechanism from that of *de novo* assembly.

Discussion

In this report, we systematically analyzed aspects of basement membrane repair in a genetically tractable system, *Drosophila* larval epidermis. Importantly, although damaged basement membrane can be repaired to a continuous sheet within 24 h after the infliction of a ~100 μm wound, this repaired sheet has a visibly altered structure that is non-uniform with respect to all four basement membrane proteins. Thus, basement membrane repairs through formation of a scar. Comparing basement membrane repair to normal growth, we find that basement membrane proteins originate from the same sources for repair and growth. However, there are some differences between repair and *de novo* assembly mechanisms. Similar to *de novo* assembly, perlecan depends on collagen IV for proper incorporation into the basement membrane scar. Yet unlike *de novo* assembly, collagen IV does not depend on laminin for its incorporation into the scar, even though similar knockdown of laminin did prevent collagen IV incorporation into new basement membranes in embryos. Though not required for collagen IV, laminin is required for the deposition of nidogen into the growing and repairing basement membrane. The dependency of nidogen on laminin *in vivo* has not been previously reported, although nidogen has been reported to bind to laminin *in vitro* [14– 16].

This is the first study we are aware of that demonstrates a scar in the basement membrane following wound repair. The basement membrane scar is characterized by increased deposition of the core basement membrane components laminin, collagen IV, perlecan, and nidogen into the repaired wound, often displaying a fibril-like appearance. The formation of a scar may explain why repaired basement membrane does not recover its full adhesive function for months following corneal wound repair [24]. It is not possible to test whether the basement membrane scar recedes over time in larvae because they undergo metamorphosis and replace the epidermis only a few hours after our experiments ended. It is possible that the presence of a continuing basement membrane scar in larvae 24h after wounding may trigger changes in gene expression in cells that contact the scar. For example, levels of the matrix remodeling protease Mmp1 remain elevated long after re-epithelialization [36], and levels of the actin binding protein Profilin remain elevated across the original wound bed even 24 h after wounding [35].

We examined the requirement for laminin, collagen IV, perlecan, and nidogen for the epidermis to close the wound, and interestingly none of these basement membrane proteins is required individually, indicating that none of these individual proteins is important as a provisional matrix for cells to migrate on during larval epidermal wound closure. A previous study showed that basement membrane is visible by electron microscopy (EM) on the basal surface of larval epidermal cells during the process of wound closure, as they migrate toward the wound, and similarly, we observe that the edge of the basement membrane appears coincident with the leading edge of the cells during wound closure. The lack of genetic requirement for wound closure, combined with the observations that matrix closes with the cells, suggests that the epidermal cells assemble the basement membrane during migration and that they migrate on the clot or cuticle on the apical side of the epidermis [25].

Although it would be easy to assume that the basement membrane components were secreted by the wound-responsive epidermal cells in a cell-autonomous manner, our data contradict that assumption. Previous studies have identified three *Drosophila* cell types that generate the protein components of basement membranes: blood cells responsible for embryonic basement membranes [28,29], fat-body cells responsible for some components of the larval imaginal disc basement membranes [19], and follicle epithelial cells responsible for reinforcing the basement membrane surrounding the growing oocyte [37,38]. We find that laminin, collagen IV, and perlecan all originate from the fat body, a distant adipose tissue. In contrast, epidermal nidogen originates from the muscles. Body wall muscles directly contact the epidermis but do not completely cover it, so that nidogen must diffuse from its cellular source like the other matrix proteins [39]. Thus, our analysis identified a fourth tissue source of basement membrane in *Drosophila*. These results indicate that, like for basement membrane growth, basement membrane repair is accomplished by utilizing soluble matrix proteins that reach damaged basement membranes simply by diffusing within the hemolymph, which bathes the basement membranes of the larval body. Interestingly, in corneal basement membrane wounds, nidogen and perlecan originate from non-epithelial stromal tissues [40], suggesting that the non-autonomy of basement membrane components is not limited to *Drosophila*.

There are many reasons to analyze basement membrane repair *in vivo*. Matrix and tissue architecture cannot easily be recapitulated in cell culture systems, and because repair is a cell non-autonomous process, it is important that all cell types of the organism are able to participate. By using *Drosophila* larvae, we have been able to capitalize on these strengths, using the flexible genetic approaches of *Drosophila* to identify source cells and requirements for assembly. However, this *in-vivo* approach has limitations as well. In order to generate a functional basement membrane before damage, we used a conditional RNAi-based knockdown strategy to deplete basement membrane components after assembly and before wounding. Because basement membrane components are secreted into hemolymph by distant tissues, we had hoped that inducing RNAi would deplete the soluble (hemolymph) fraction of protein while sparing the insoluble (assembled) fraction. A significant portion of each larval matrix protein is soluble, as indicated by fractionating control lysates followed by western blotting. However, western blots showed that the insoluble fractions were significantly reduced after knockdown, ranging from 67% loss (collagen IV) to 93% loss (perlecan). The reduction of protein from the assembled basement membrane no doubt represents “thinning” of basement membranes due to continued matrix growth over two days of knockdown, and the reduction may be augmented by a concentration-dependent disassembly of insoluble basement membrane to restore the soluble portion. If soluble protein is released from deposited basement membranes, it would generate a pool of available protein in the hemolymph that cannot be experimentally eliminated, in addition to the inherent leakiness of RNAi that allows a small amount of continued protein synthesis. Free exchange between polymerized basement membrane protein and soluble subunits seems especially reasonable for laminin, which is polymerized via many weak interactions [41]. It is possible that exchange of subunits between soluble and deposited basement membrane may explain the second minor source of laminin and/or perlecan in epidermal growth, and this pool may also contribute to basement membrane repair after wounding.

The observation that the organization of perlecan within the repaired wound is altered in the absence of collagen IV is similar to previous studies showing that collagen IV is required for perlecan deposition during the growth of several larval basement membranes [19]. However, the phenotype we observed was subtly different: in the absence of collagen IV, perlecan was present within the repaired basement membrane but its appearance was altered. The heparan sulfate chains that characterize heparan sulfate proteoglycans like perlecan can interact with hundreds of different proteins [42]. It is possible that the absence of collagen IV from the repaired basement membrane liberates perlecan to bind non-specifically with other molecules, creating the fluorescent haze we observed around wounds repaired in the absence of collagen IV. Alternatively, perlecan may bind specifically to multiple basement membrane proteins *in vivo*.

It was surprising to find that collagen IV deposition is not sensitive to laminin levels in the repaired wound. This lack of dependency stands in contrast to data showing laminin to be crucial for collagen IV deposition in the developing embryo [12,13]. The difference in wound repair may be that collagen IV is already present in the epidermal basement membrane prior to the depletion of laminin. Upon laminin depletion, collagen IV is maintained outside the wound borders after laminin knockdown. This assembled collagen IV matrix may provide scaffolding from which newly deposited collagen IV can self-assemble, extending into the repaired wound independently of laminin. In contrast, the deposition of nidogen into the basement membrane scar appeared to be entirely dependent on the presence of laminin. Though nidogen has been shown to bind laminin, collagen IV, and perlecan [43], our analysis indicates that laminin is the crucial component for nidogen recruitment into the basement membrane scar.

Experimental Procedures

Fly husbandry

Flies were maintained on cornmeal-molasses media supplemented with dry yeast. Flies are listed in Table 1. For all experiments with GFP-labeled BM proteins, flies contained a single copy of the GFP-labeled protein. For basement membrane source experiments, crosses were carried out at 25°C (Fig. 8A). For functional experiments requiring conditional knockdown with *Gal4/Gal80^{ts}*, including basement membrane order of assembly experiments, the following conditions were used: for *LanB1, vkg*, and *trol* knockdown experiments, parents were allowed to pre-mate for 2–3 days at 18°C (permissive temperature) and then moved to fresh bottles to lay for 24 h at 18°C. Parents were removed and embryos developed an additional 24 h at 18°C for *LanB1* and *trol* knockdown experiments, or for an additional 48 h for *vkg* knockdown experiments. Bottles were then shifted to 29°C (knockdown conditions) and larvae developed to the foraging 3rd instar stage, approximately 4 days for *LanB1* and *trol* knockdown experiments and 3.5 days for *vkg* knockdown experiments (Fig. 8B). 3rd instar larvae were identified by branching of the anterior spiracles. For *Ndg* knockdown experiments, crosses and progeny were maintained at 29°C.

Epidermal Pinch-Wounding

Third-instar larvae were pinched on the dorsal side between the hair stripes segments A3 and A4 for approximately 10 sec with blunted #5 dissecting forceps (Dumont), as adapted from Galko and Krasnow (2004). Care was taken to not puncture the cuticle. However, in *Tub>dsRNA*^{LanB1} larvae the cuticle was more easily damaged than in other larvae, leading to small areas of melanization, which autofluoresce in the green channel. Melanization was most visible when Ndg-GFP was imaged (see Fig. 6Q) because the GFP signal is particularly faint in the *LanB1* knockdown. After wounding, larvae recovered on grape juice plates, with access to wet yeast, for 24 h. If larvae were raised at 29°C, then recovery from wounding was also at 29°C; otherwise recovery was at 25°C.

Larval dissection, fixation, and immunohistochemistry

Larvae were decapitated at the cerebral tracheal branch in chilled PBS and filleted along the ventral side. Dissections were performed in PBS + 4% paraformaldehyde, and immediately larval pelts were pinned flat and fixed for 20 min. Samples were washed at room temperature (RT) in PBS + 0.2% Triton X-100 (PBT-X), 2X 5 min. each and 1× 30 min. The pelts were blocked in PBT-X + 5% normal goat serum + 0.02% NaN_3 for 3 h at RT and then incubated in 1° antibodies overnight at 4°C. The following day, pelts were washed twice in PBT-X (1 h per wash) at RT followed by incubation in 2° antibodies for 2 h at RT. Lastly, they were washed in PBT-X for 2 h at RT and quickly washed in PBS prior to mounting on glass slides in Vectashield mounting media with DAPI (Vector Laboratories, Burlingame, CA). For antibodies, rabbit Anti-GFP (Torrey Pines Biolabs, Secaucus, NJ, catalog number TP401) was used at a 1:200 dilution for imaging Vkg-GFP, Trol-GFP and LanB1-GFP. For imaging Ndg-GFP, Rabbit Anti-GFP (Abcam, catalog number ab6556) was used at a 1:1000 dilution. For imaging FasIII, Mouse 7G10 Anti-FasIII (Developmental Studies Hybridoma Bank, Iowa City, IA) was used at a 1:10 dilution. Secondary antibodies (Jackson Immunoresearch Laboratories, West Grove, PA) were FITC Donkey Anti-Rabbit (code number 711–095-152) and Cy3 Goat Anti-Mouse (code number 115–165-206), each used at 1:500.

Gal4 Driver Characterization

Gal4 drivers were used to constitutively express GFP in each of the candidate tissues tested. Upon reaching the 3rd instar stage, larvae were dissected and fixed as described above. The entire animal carcass was inspected for GFP expression, with special attention paid to the epidermis, muscles, and fat body. Exposure levels were kept the same between tissues of the same animal in Fig. S2A-D. For *Hml-Gal4* expression, intact larvae were imaged to prevent loss of hemocytes upon dissection.

Microscopy

To image larval pelts and fixed embryos, optical sections were taken using a Zeiss Apotome mounted to an Axio Imager M2 using the following objectives: 10x/0.3 EC Plan-NeoFluar, 20x/0.8 Plan-Apochromat, or 40x/1.3 EC Plan-NeoFluar. Images were acquired with an AxioCam MRm (Zeiss, Thornwood, NY) camera, X-Cite 120Q light source (Excelitas Technologies, Waltham, MA) and AxioVision 4.8 (Zeiss) software. All stacks were exported

to ImageJ, version 1.48v (National Institutes of Health, Bethesda, MD), as 16-bit, grayscale, ZVI files for analysis. For basement membrane source experiments in unwounded larvae, exposure levels were matched to control samples imaged on the same day. For all other experiments, exposure levels were optimized independently. For live embryos, images were acquired with a Zeiss Axiocam MRc camera mounted to a Zeiss Lumar V12 stereomicroscope, using a Neolumar S 1.5x objective, X-Cite 120Q light source and Axiovision 4.8 software. Images were exported to ImageJ version 1.48v, as 8-bit TIFF files, for analysis.

Mean fluorescence intensity measurements and analysis

For basement membrane source experiments (Fig. 3), knock-down animals were always stained for GFP simultaneously with control animals (no knockdown). After staining, a representative region of basement membrane was imaged for each larva by compiling optical sections into a maximum projection, saved as a TIFF file in ImageJ 1.48v software. The ImageJ Measure tool was used to record mean fluorescence intensity for each animal from representative X-Y regions of basement membrane, selected by the absence of obscuring tissue or tears. The mean intensity for each animal was imported into Microsoft Excel and normalized to the mean of the control (no knockdown) samples that were stained simultaneously. Normalizing the mean fluorescence for each larva allowed fluorescence to be compared between experiments without concern for fluctuations in illumination intensity or antibody batches. Normalized data was imported into GraphPad Prism 7.0d and an ANOVA test was used to determine statistical significance among all datasets. An unpaired t-test coupled with a Bonferroni correction was then used to determine significance between two data sets of interest. For these experiments Trol-GFP was analyzed only in female larvae because of dosage compensation on the X chromosome.

For wounded samples (Fig. 4), mean fluorescence was measured from max projections in the repaired region (defined by the indentation of the cuticle following pinch-wounding) and in a representative unwounded region within the same image. The ratio between the two measurements for each sample was then calculated in Excel, and the ratio data was plotted and analyzed in GraphPad. Unpaired t-tests were used to determine significance between control and experimental datasets.

For embryo samples (Fig. 7), images were imported into ImageJ version 1.48v and the Measure tool was used to measure average fluorescence intensity of whole embryos. An ANOVA test was used to determine statistical significance among all data sets, followed by unpaired t-tests coupled with a Bonferroni correction to determine significance between specific data sets.

Fluorescence anisotropy measurements and analysis

Using ImageJ, optical sections were compiled into maximum projections and saved as TIFF files for analysis. Because the least fluorescence within a repaired wound area was found underneath the nuclei, we calculated the mean fluorescence under the nuclei by tracing the nuclei within the cuticle-indentation borders (marking the wound) and calculating the mean fluorescence within these sub-nuclear regions. To reproducibly identify the maximal

intensity of basement membrane deposition within the wound, we used the Threshold and Measure tools to record the mean of the top 5% of pixel values. Fluorescence anisotropy within the repaired wound was calculated as the ratio of the top 5% pixel values over the subnuclear fluorescence. This ratio was imported into GraphPad Prism 7.0d and an ANOVA test was used determine statistical difference among all datasets. Unpaired t-tests coupled with a Bonferroni correction were used to determine significance between specific datasets.

Embryo collection, fixation, and immunohistochemistry

Fattened females were allowed to lay eggs on grape juice-agar plates with wet yeast at 29°C for 4 h, and embryos were aged at 29°C for 9–10 h. To collect embryos for live measurement of LanB1-GFP fluorescence, embryos were rinsed into a beaker with 50% bleach and swirled for 2 min. to remove the chorion and then washed with water and gently blotted dry, then transferred to grape plates and immediately imaged on a fluorescence stereomicroscope (see above). *LanB1-GFP, tub-Gal4/+; UAS-dsRNA^{LanB1}* were compared to siblings lacking *UAS-dsRNA^{LanB1}*, identified by the presence or absence of the red balancer *TM3, sChFP.*

To analyze Vkg-GFP assembly along the ventral nerve cord when *LanB1* was constitutively knocked down in embryos, embryos of genotype *vkgGFP^{205}/+; TubGal4/UAS-dsRNA^{LanB1}* were compared to *vkgGFP^{205}/+; TubGal4/+*. Embryos were laid and aged as above. For fixation, embryos were transferred into 2 ml of 100% heptane in a glass vial. Next, 2 ml of 16% formaldehyde was added to the vial, bringing the embryos to the interface between heptane and formaldehyde, and the vial was shaken for 10 min. The formaldehyde and heptane were removed and replaced with 5 ml of fresh 100% heptane. To remove the vitelline membrane, 5 ml of 100% methanol was added and the vial was immediately shaken vigorously by hand for 30 s. The heptane and methanol were removed and replaced with 2 ml fresh methanol and transferred to an Eppendorf tube. Embryos were rehydrated and washed twice in PBS + 0.2% Triton X-100 (PBT-X) and blocked in 1% bovine serum albumin (BSA) in PBT-X for 1 h on a rocker at RT. For imaging Vkg-GFP, mouse anti-GFP antibodies (UC Davis catalog # 73–131 and # 73–132) were used at a 1:5 dilution, rocking overnight at 4°C. The following day, embryos were washed in PBT-X three times for 30 min each, rocking at RT. Next, embryos were incubated in FITC Goat anti-Mouse (Jackson Immunoresearch Laboratories, West Grove, PA, code number 115–095-206) diluted 1:500 for 3 h rocking at RT. Finally, embryos were washed three times in PBT-X for 30 min each and once in PBS. All PBS was removed and embryos were resuspended in Vectashield mounting media with DAPI (Vector Laboratories, Burlingame, CA) prior to being mounted on a glass slide. To assess collagen IV assembly into basement membranes around the ventral nerve cord, stage 16–17 embryos were identified by gut morphology. *LanB1* knockdown embryos were identified by the absence of an mCherry balancer. The knockdown embryos were extremely fragile, and 3 intact embryos were identified. Collagen IV was not assembled along the ventral nerve cord grooves in any of them.

Western Blots

From 10–100 3rd-instar larvae were frozen in liquid nitrogen and ground to a powder with a mortar and pestle; each larva yielded ~1 mg powder. The powder was re-suspended to a concentration of 50 mg/ml in ice-cold RIPA buffer (10 mM Tris-Cl pH = 8.0, 1 mM EDTA,

1% Triton X-100, 0.1% sodium deoxycholate, 0.1% SDS, 140 mM NaCl) plus 1x HALT protease inhibitor cocktail (Thermo Scientific). Samples were centrifuged for 15 min at 4°C at 16,110 x g. The supernatant, containing the soluble fraction, was removed and mixed with Laemmli sample buffer (1X). The pellet, containing the insoluble fraction, was washed 3X in 1 ml chilled RIPA buffer per 75 mg original powder, and resuspended to 50 mg/ml by vortexing in RIPA buffer. The pellet suspension was mixed with Laemmli sample buffer (2X final concentration). Samples were boiled for 5 min. and spun for 30 s at 16,110 x g. 15–30 μl (equivalent to about 1 larva) was loaded onto either 10% or 4–20% SDS PAGE gels (Bio-Rad Laboratories), transferred to nitrocellulose (GE Healthcare) and incubated with 1° antibodies overnight at 4°C followed by 2º antibody incubation (Li-Cor) at 1:2000 for 1 h at RT. Blots were developed and imaged with the Odyssey Infrared Imaging System (Li-Cor Biosciences). The 1° antibodies used to detect GFP were Rabbit anti-GFP (Torrey Pines Biolabs, Secaucus, NJ, catalog number TP401) at a dilution of 1:1000 or Rabbit anti-GFP (Abcam, catalog number ab6556) at a dilution of 1:1000. Antibodies used for loading controls were Mouse anti-Actin (EMD Millipore, catalog number MAB1501R) at a dilution of 1:2000 and Goat Anti-GAPDH (Imgenex, catalog number #IMG3073) at a dilution of 1:2500). Actin was used as the loading control for the insoluble fraction while GAPDH was used as the loading control for the soluble fraction.

Supplementary Material

Refer to Web version on PubMed Central for supplementary material.

Acknowledgements

The authors wish to thank Gautam Bhave for help and guidance with fractionating and blotting matrix proteins, and we thank Guy Tanentzapf for locating GFP-fusion fly lines. We thank Sally Horne-Badovinac, the Bloomington Drosophila Stock Center, and the Vienna Drosophila RNAi Center for fly stocks; and the Developmental Studies Hybridoma Bank for antibodies. We thank Kimi LaFever, Indrayani Waghmare, and Angela Howard for comments on the manuscript. This work was supported by the National Institutes of Health 5R01GM073883 and R21AR072510 to APM.

References

[1]. Fidler AL, Darris CE, Chetyrkin SV, Pedchenko VK, Boudko SP, Brown KL, et al., Collagen IV and basement membrane at the evolutionary dawn of metazoan tissues, Elife 6 (2017) 1–24. 10.7554/eLife.24176.

[2]. Pozzi A, Yurchenco PD, Iozzo RV, The nature and biology of basement membranes, Matrix Biology 57–58 (2017) 1–11. 10.1016/j.matbio.2016.12.009.

[3]. Wang X, Harris RE, Bayston LJ, Ashe HL, Type IV collagens regulate BMP signalling in Drosophila, Nature 455 (2008) 72–77. 10.1038/nature07214. [PubMed: 18701888]

[4]. Ma M, Cao X, Dai J, Pastor-Pareja JC, Basement Membrane Manipulation in Drosophila Wing Discs Affects Dpp Retention but Not Growth Mechanoregulation, Developmental Cell 42 (2017) 97–106.e4. 10.1016/j.devcel.2017.06.004. [PubMed: 28697337]

[5]. Skeath JB, Wilson BA, Romero SE, Snee MJ, Zhu Y, Lacin H, The extracellular metalloprotease AdamTS-A anchors neural lineages in place within and preserves the architecture of the central nervous system, Development 144 (2017) 3102–3113. 10.1242/dev.145854. [PubMed: 28760813]

[6]. Crest J, Diz-Muñoz A, Chen D-Y, Fletcher DA, Bilder D, Organ sculpting by patterned extracellular matrix stiffness, Elife 6 (2017) 1–16. 10.7554/eLife.24958.

[7]. Chlasta J, Milani P, Runel G, Duteyrat JL, Arias L, Lamire LA, et al., Variations in basement membrane mechanics are linked to epithelial morphogenesis, Development 144 (2017) 4350–4362. 10.1242/dev.152652. [PubMed: 29038305]

[8]. Bhave G, Colon S, Ferrell N, The sulfilimine cross-link of collagen IV contributes to kidney tubular basement membrane stiffness, American Journal of Physiology-Renal Physiology 313 (2017) F596–F602. 10.1152/ajprenal.00096.2017. [PubMed: 28424209]

[9]. Ramos-Lewis W, Page-McCaw A, Basement membrane mechanics shape development: Lesson from the fly, Matrix Biology (2018). 10.1016/j.matbio.2018.04.004.

[10]. Li S, Qi Y, McKee K, Liu J, Hsu J, Yurchenco PD, Integrin and dystroglycan compensate each other to mediate laminin-dependent basement membrane assembly and epiblast polarization, Matrix Biology 57–58 (2017) 272–284. 10.1016/j.matbio.2016.07.005.

[11]. Yurchenco PD, Furthmayr H, Self-assembly of basement membrane collagen, Biochemistry 23 (1984) 1839–1850. 10.1021/bi00303a040. [PubMed: 6722126]

[12]. Pöschl E, Schlotzer-Schrehardt U, Brachvogel B, Saito K, Ninomiya Y, Mayer U, Collagen IV is essential for basement membrane stability but dispensable for initiation of its assembly during early development, Development 131 (2004) 1619–1628. 10.1242/dev.01037. [PubMed: 14998921]

[13]. Urbano JM, Torgler CN, Molnar C, Tepass U, Lopez-Varea A, Brown NH, et al., Drosophila laminins act as key regulators of basement membrane assembly and morphogenesis, Development 136 (2009) 4165–4176. 10.1242/dev.044263. [PubMed: 19906841]

[14]. Fox JW, Mayer U, Nischt R, Aumailley M, Reinhardt D, Wiedemann H, et al., Recombinant nidogen consists of three globular domains and mediates binding of laminin to collagen type IV, The EMBO Journal 10 (1991) 3137–3146. 10.1002/j.1460-2075.1991.tb04875.x. [PubMed: 1717261]

[15]. Ries A, Göhring W, Fox JW, Rupert T, Sasaki T, Recombinant domains of mouse nidogen-1 and their binding to basement membrane proteins and monoclonal antibodies, European Journal of Biochemistry (2001) 1–10. [PubMed: 11121095]

[16]. Takagi J, Yang Y, Liu J-H, Wang J-H, Springer TA, Complex between nidogen and laminin fragments reveals a paradigmatic β-propeller interface, Nature 424 (2003) 969–974. 10.1038/nature01899. [PubMed: 12931195]

[17]. Gubbiotti MA, Neill T, Iozzo RV, A current view of perlecan in physiology and pathology: A mosaic of functions, Matrix Biology 57–58 (2017) 285–298. 10.1016/j.matbio.2016.09.003.

[18]. Hopf M, Göhring W, Kohfeldt E, Yamada Y, Timpl R, Recombinant domain IV of perlecan binds to nidogens, laminin–nidogen complex, fibronectin, fibulin-2 and heparin, European Journal of Biochemistry 259 (1999) 917–926. 10.1046/j.1432-1327.1999.00127.x. [PubMed: 10092882]

[19]. Pastor-Pareja JC, Xu T, Shaping Cells and Organs in Drosophila by Opposing Roles of Fat Body-Secreted Collagen IV and Perlecan, Developmental Cell 21 (2011) 245–256. 10.1016/j.devcel.2011.06.026. [PubMed: 21839919]

[20]. Amano S, Possible Involvement of Basement Membrane Damage in Skin Photoaging, Journal of Investigative Dermatology 14 (2009) 2–7. 10.1038/jidsymp.2009.5. [PubMed: 19675545]

[21]. Miner JH, The glomerular basement membrane, Exp. Cell Res 318 (2012) 973–978. 10.1016/j.yexcr.2012.02.031. [PubMed: 22410250]

[22]. Marino GK, Santhiago MR, Santhanam A, Torricelli AAM, Wilson SE, Regeneration of Defective Epithelial Basement Membrane and Restoration of Corneal Transparency After Photorefractive Keratectomy, J Refract Surg 33 (2017) 337–346. 10.3928/1081597X-20170126-02. [PubMed: 28486725]

[23]. Fujikawa LS, Foster CS, Gipson IK, Colvin RB, Basement membrane components in healing rabbit corneal epithelial wounds: immunofluorescence and ultrastructural studies, The Journal of Cell Biology 98 (1984) 128–138. [PubMed: 6368566]

[24]. Khodadoust AA, Silverstein AM, Kenyon KR, Dowling JE, Adhesion of regenerating corneal epithelium, American Journal of Ophthalmology 65 (1968) 339–348. 10.1016/0002-9394(68)93082-1. [PubMed: 5640539]

[25]. Galko MJ, Krasnow MA, Cellular and Genetic Analysis of Wound Healing in Drosophila Larvae, Plos Biol 2 (2004) 1114–1126. 10.1371/journal.pbio.0020239.

[26]. Sarov M, Barz C, Jambor H, Hein MY, Schmied C, Suchold D, et al., A genome-wide resource for the analysis of protein localisation in Drosophila, Elife 5 (2016) e12068 10.7554/eLife.12068. [PubMed: 26896675]

[27]. Glasheen BM, Robbins RM, Piette C, Beitel GJ, Page-McCaw A, A matrix metalloproteinase mediates airway remodeling in Drosophila, Developmental Biology 344 (2010) 772–783. 10.1016/j.ydbio.2010.05.504. [PubMed: 20513443]

[28]. Fessler JH, Fessler LI, Drosophila extracellular matrix, Annu. Rev. Cell Biol 5 (1989) 309–339. 10.1146/cellbio.1989.5.issue-1;page:string:Article/Chapter. [PubMed: 2557060]

[29]. Matsubayashi Y, Louani A, Dragu A, Sánchez-Sánchez BJ, Serna-Morales E, Yolland L, et al., A Moving Source of Matrix Components Is Essential for De Novo Basement Membrane Formation, Current Biology 27 (2017) 3526– 3534. 10.1016/j.cub.2017.10.001. [PubMed: 29129537]

[30]. Babcock DT, Brock AR, Fish GS, Wang Y, Perrin L, Krasnow MA, et al., Circulating blood cells function as a surveillance system for damaged tissue in Drosophila larvae, Proc. Natl. Acad. Sci. U.S.A 105 (2008) 10017–10022. 10.1073/pnas.0709951105. [PubMed: 18632567]

[31]. Jung M, Lord MS, Cheng B, Lyons JG, Alkhouri H, Hughes JM, et al., Mast cells produce novel shorter forms of perlecan that contain functional endorepellin: a role in angiogenesis and wound healing, Journal of Biological Chemistry 288 (2013) 3289–3304. 10.1074/jbc.M112.387811. [PubMed: 23235151]

[32]. Gramates LS, Marygold SJ, Santos GD, Urbano J-M, Antonazzo G, Matthews BB, et al., FlyBase at 25: looking to the future, Nucleic Acids Research 45 (2017) D663–D671. 10.1093/nar/gkw1016. [PubMed: 27799470]

[33]. Kelemen-Valkony I, Kiss M, Csiha J, Kiss A, Bircher U, Szidonya J, et al., Drosophila basement membrane collagen col4a1 mutations cause severe myopathy, Matrix Biology 31 (2012) 29–37. 10.1016/j.matbio.2011.09.004. [PubMed: 22037604]

[34]. Voigt A, Pflanz R, Schäfer U, Jäckle H, Perlecan participates in proliferation activation of quiescent Drosophila neuroblasts, Developmental Dynamics 224 (2002) 403–412. 10.1002/dvdy.10120. [PubMed: 12203732]

[35]. Brock AR, Wang Y, Berger S, Renkawitz-Pohl R, Han VC, Wu Y, et al., Transcriptional regulation of Profilin during wound closure in Drosophila larvae, Journal of Cell Science 125 (2013) 5667–5676. 10.1242/jcs.107490.

[36]. Stevens LJ, Page-McCaw A, A secreted MMP is required for reepithelialization during wound healing, Molecular Biology of the Cell 23 (2012) 1068–1079. 10.1091/mbc.E11-09-0745. [PubMed: 22262460]

[37]. Denef N, Chen Y, Weeks SD, Barcelo G, Schüpbach T, Crag Regulates Epithelial Architecture and Polarized Deposition of Basement Membrane Proteins in Drosophila, Developmental Cell 14 (2008) 354–364. 10.1016/j.devcel.2007.12.012. [PubMed: 18331716]

[38]. Isabella AJ, Horne-Badovinac S, Rab10-Mediated Secretion Synergizes with Tissue Movement to Build a Polarized Basement Membrane Architecture for Organ Morphogenesis, Developmental Cell 38 (2016) 47–60. 10.1016/j.devcel.2016.06.009. [PubMed: 27404358]

[39]. Galindo RL, Allport JA, Olson EN, A Drosophila model of the rhabdomyosarcoma initiator PAX7-FKHR, Proc. Natl. Acad. Sci. U.S.A 103 (2006) 13439–13444. 10.1073/pnas.0605926103. [PubMed: 16938866]

[40]. Torricelli AAM, Marino GK, Santhanam A, Wu J, Singh A, Wilson SE, Epithelial basement membrane proteins perlecan and nidogen-2 are up-regulated in stromal cells after epithelial injury in human corneas, Experimental Eye Research 134 (2015) 33–38. 10.1016/j.exer.2015.03.016. [PubMed: 25797478]

[41]. Hussain SA, Carafoli F, Hohenester E, Determinants of laminin polymerization revealed by the structure of the α5 chain amino-terminal region, EMBO Reports 12 (2011) 276–282. 10.1038/embor.2011.3. [PubMed: 21311558]

[42]. Rabenstein DL, Heparin and heparan sulfate: structure and function, Nat. Prod. Rep 19 (2002) 312–331. 10.1039/b100916h. [PubMed: 12137280]

[43]. Yurchenco PD, Basement Membranes: Cell Scaffoldings and Signaling Platforms, Cold Spring Harbor Perspectives in Biology 3 (2011) 1–27. 10.1101/cshperspect.a004911.

[44]. Buszczak M, Paterno S, Lighthouse D, Bachman J, Planck J, Owen S, et al., The Carnegie Protein Trap Library: A Versatile Tool for Drosophila Developmental Studies, Genetics 175 (2006) 1505–1531. 10.1534/genetics.106.065961. [PubMed: 17194782]

[45]. Kelso RJ, Buszczak M, Quinones AT, Castiblanco C, Mazzalupo S, Cooley L, Flytrap, a database documenting a GFP protein-trap insertion screen in Drosophila melanogaster, Nucleic Acids Research 32 (2004) D418–D420. 10.1093/nar/gkh014. [PubMed: 14681446]

[46]. Page-McCaw A, Serano J, Santé JM, Rubin GM, Drosophila Matrix Metalloproteinases Are Required for Tissue Remodeling, but Not Embryonic Development, Developmental Cell 4 (2003) 95–106. 10.1016/S1534-5807(02)00400-8. [PubMed: 12530966]

Highlights

- Basement membrane forms a scar during wound repair in *Drosophila* larvae.
- Epidermal basement membrane originates from adipose tissue and muscle in *Drosophila* larvae.
- Collagen IV recruitment to the repairing basement membrane does not require laminin.
- Nidogen recruitment to the repairing basement membrane requires laminin.

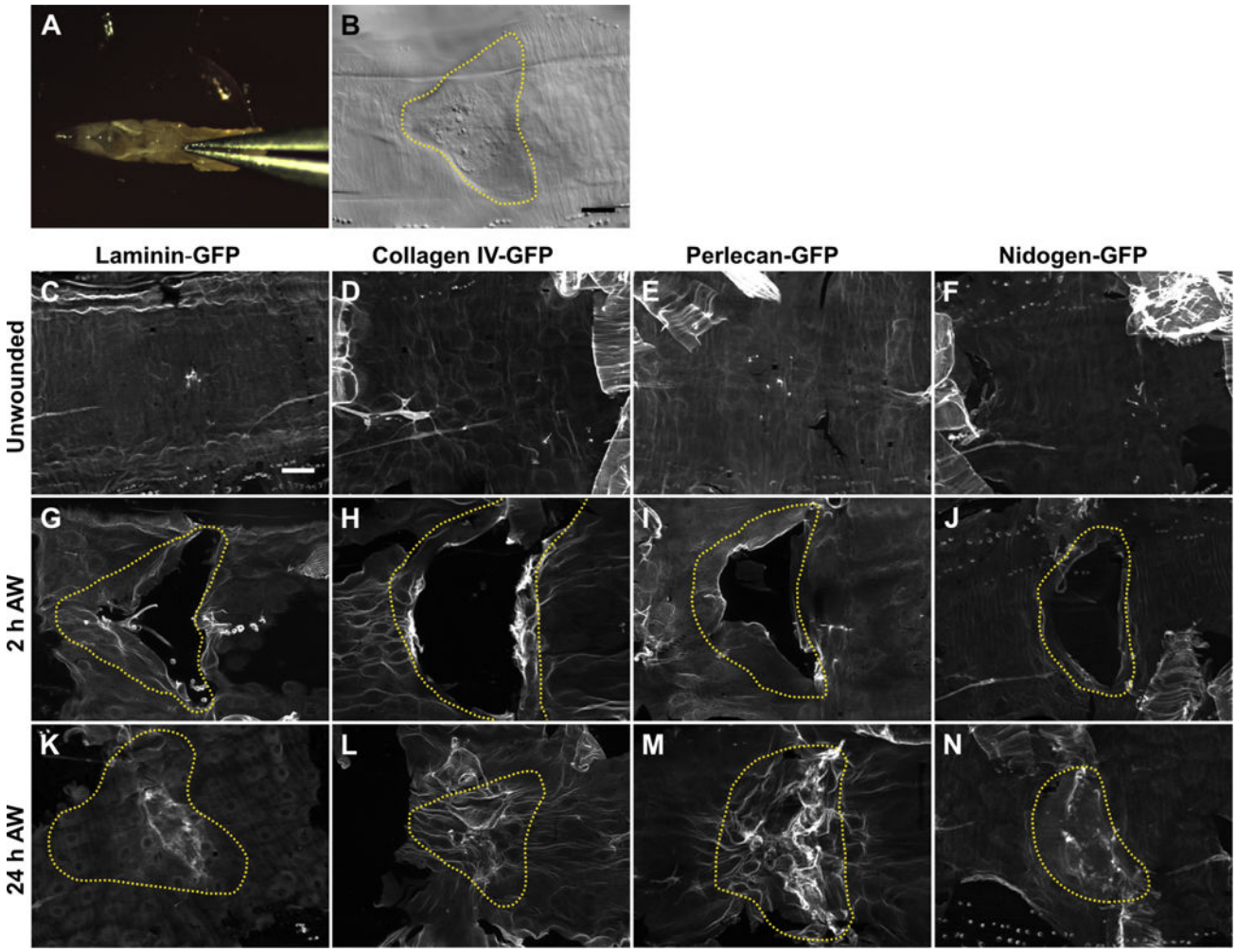

Figure 1: The basement membrane is damaged by pinch wounds and forms a scar upon repair.

A) To damage the basement membrane, blunt forceps were used to pinch larvae on the dorsal epidermis between the hair stripes of segments A3 and A4. **B)** Pinch wounds do not break the outer cuticle, but they do leave an indentation visible with DIC, outlined with yellow dotted line. **C-F)** Undamaged epidermal basement membrane visualized with GFP-fusion constructs of each of the core basement membrane proteins. Images are representative of the no-knockdown controls quantified in Fig. 3. **G-J)** Damaged epidermal basement membrane after pinch-wounding. **K-N)** Within 24 h, the basement membrane was repaired, leaving behind a visible scar in the region of the healed wound. Images are representative of the no-knockdown controls quantified in Fig. 4. Dotted yellow lines indicate original wound borders based on cuticle indentation. Scale bar, 50 μm.

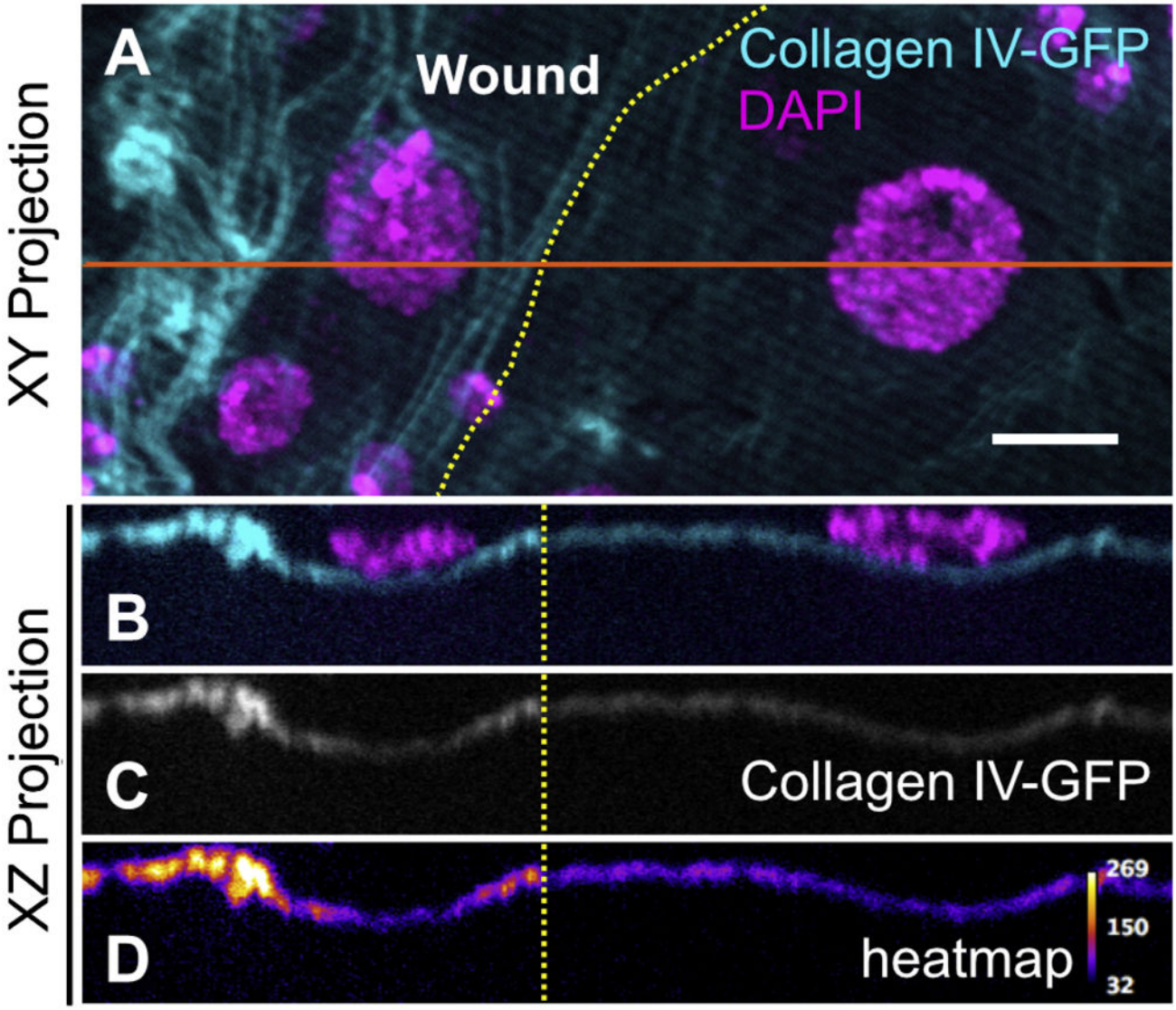

Figure 2: The basement membrane scar is thicker than unwounded basement membrane.

Yellow dotted lines indicate wound border. Orange solid line indicates location sampled for XZ projections. **A)** Basement membrane scar, evident on the left (wounded) side. **B-D)** Z-section shows increased thickness and fluorescence of collagen IV within the healed wound ($N \geq 3$). Scale bar, 10μm.

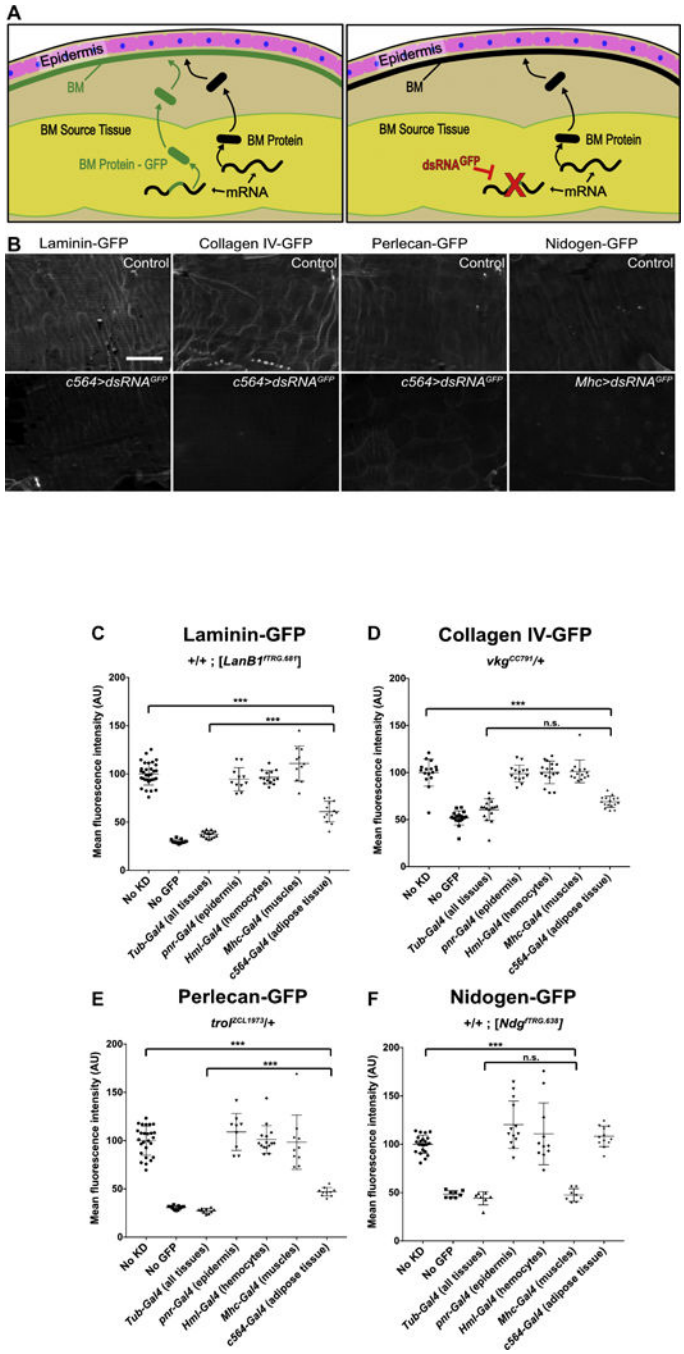

Figure 3: In unwounded epidermis, basement membrane proteins come from other tissues.

A) Experiment overview: tissue expressing a basement membrane protein allele fused to GFP (BM-GFP) and an allele not fused with GFP will secrete both forms for incorporation into the basement membrane, resulting in fluorescent basement membrane. When *dsRNA*^{GFP} targets GFP in the source tissue, only the basement membrane protein lacking GFP will be secreted, resulting in non-fluorescent basement membrane. **B)** Example images without (top) and with (bottom) *dsRNA*^{GFP} expression. Scale bar, 50 μm. **C-E)** Laminin-GFP, collagen IV-GFP, or perlecan-GFP is lost from the epidermal BM when *dsRNA*^{GFP} is

expressed in adipose tissue. **F)** Nidogen-GFP is lost from the epidermal BM when $dsRNA^{GFP}$ is expressed in the muscles. *** indicates $p \leq 0.001$.

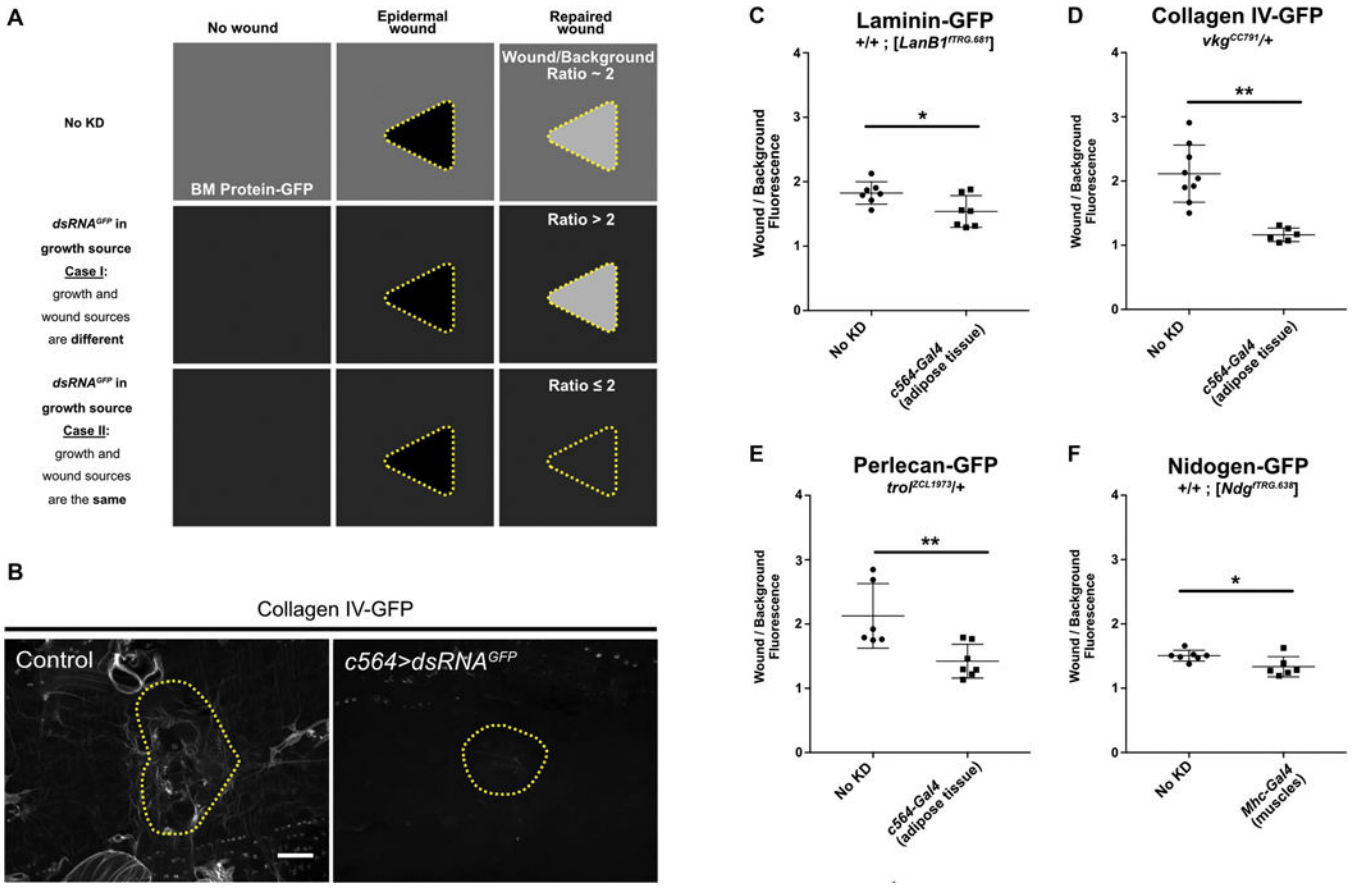

Figure 4: The sources of basement membrane for repairing damage are the same as for growth.

A) Schematic of possible outcomes to test for a wound-specific source of basement membrane. In control unwounded epidermis, the basement membrane is fluorescent (depicted as medium gray color, top left) from the incorporation of BM-GFP. After repair, the basement membrane in the wound area is about 2-fold brighter than background (top right). If the tissue sources for growth (unwounded) and repair of basement membrane are different, then the permanent knockdown of GFP in the growth source tissue will cause the intact basement membrane (background) to become dim, but the repaired area is expected to remain bright, increasing the wound/background ratio. If the tissue source for growth (unwounded) and repair is the same, the permanent knockdown of GFP in the source tissue is expected to affect basement membrane repair in a similar manner, maintaining or reducing the wound/background ratio. **B)** Example of repaired epidermal basement membrane in the absence of $dsRNA^{GFP}$ (left) or in the presence of $dsRNA^{GFP}$ expressed in the fat body (right). **C-F)** Ratio of average fluorescence inside the wound over outside the wound with or without $dsRNA^{GFP}$ expression in the growth source tissue for epidermal basement membrane. Components appear to come from the same source tissues for growth and repair of basement membrane. * indicates $p \leq 0.05$, ** indicates $p \leq 0.01$. Scale bar, 50 μm.

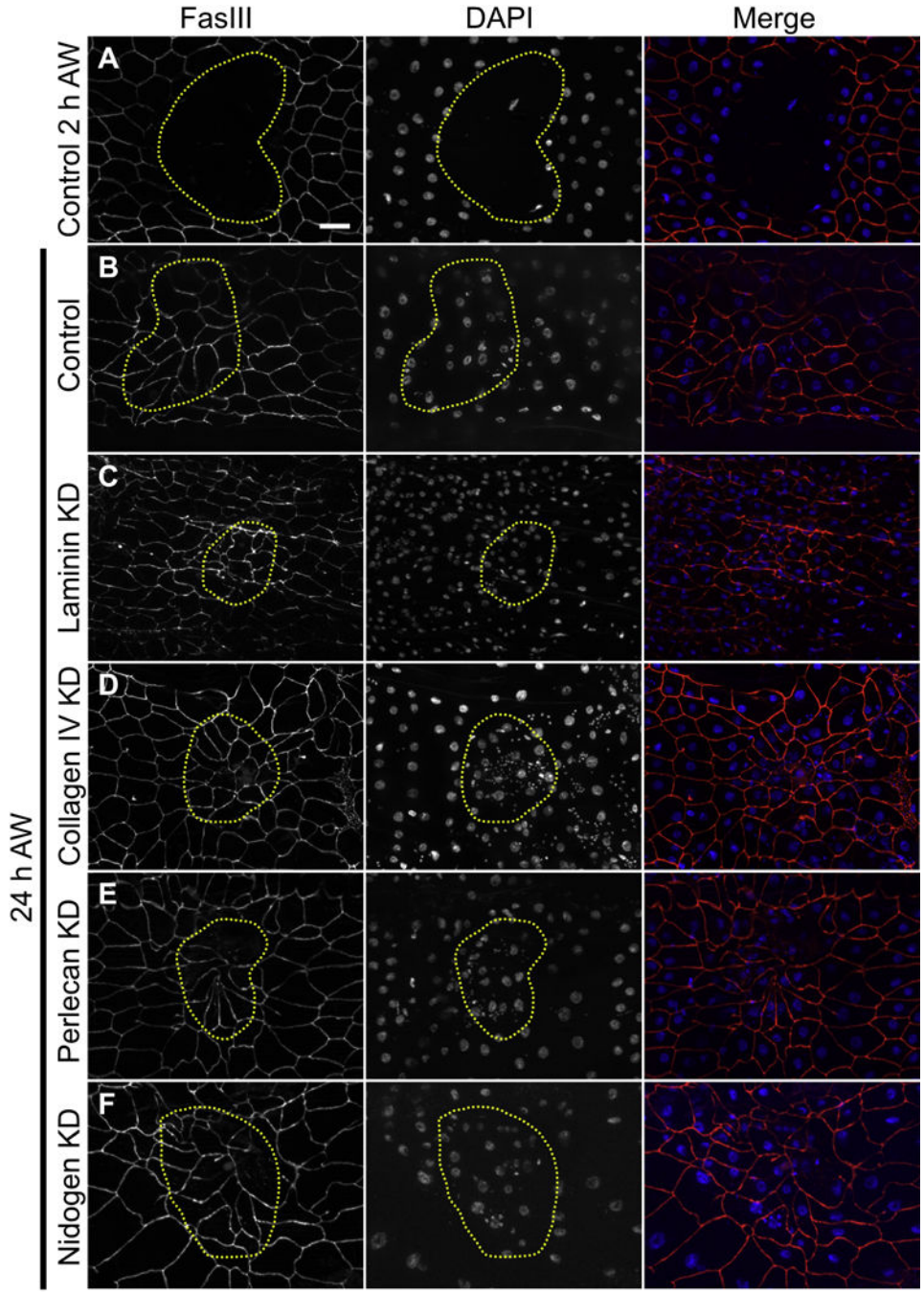

Figure 5: Cells do not require any of the core basement membrane proteins to close wounds.
A) 2 h after injury, wounds were open. **B-F)** 24 h after injury, cells had closed the wound in (**B**) controls, or (**C-F**) when laminin, collagen IV, perlecan, or nidogen was knocked down days before wounding. Note that multinucleate syncytial cells were present after repair in control as well as knockdown wounds as previously reported [25]. Panels A-F are representative of 7, 25, 16, 15, 18, and 14 wounds examined, respectively. Scale bar, 50 μm.

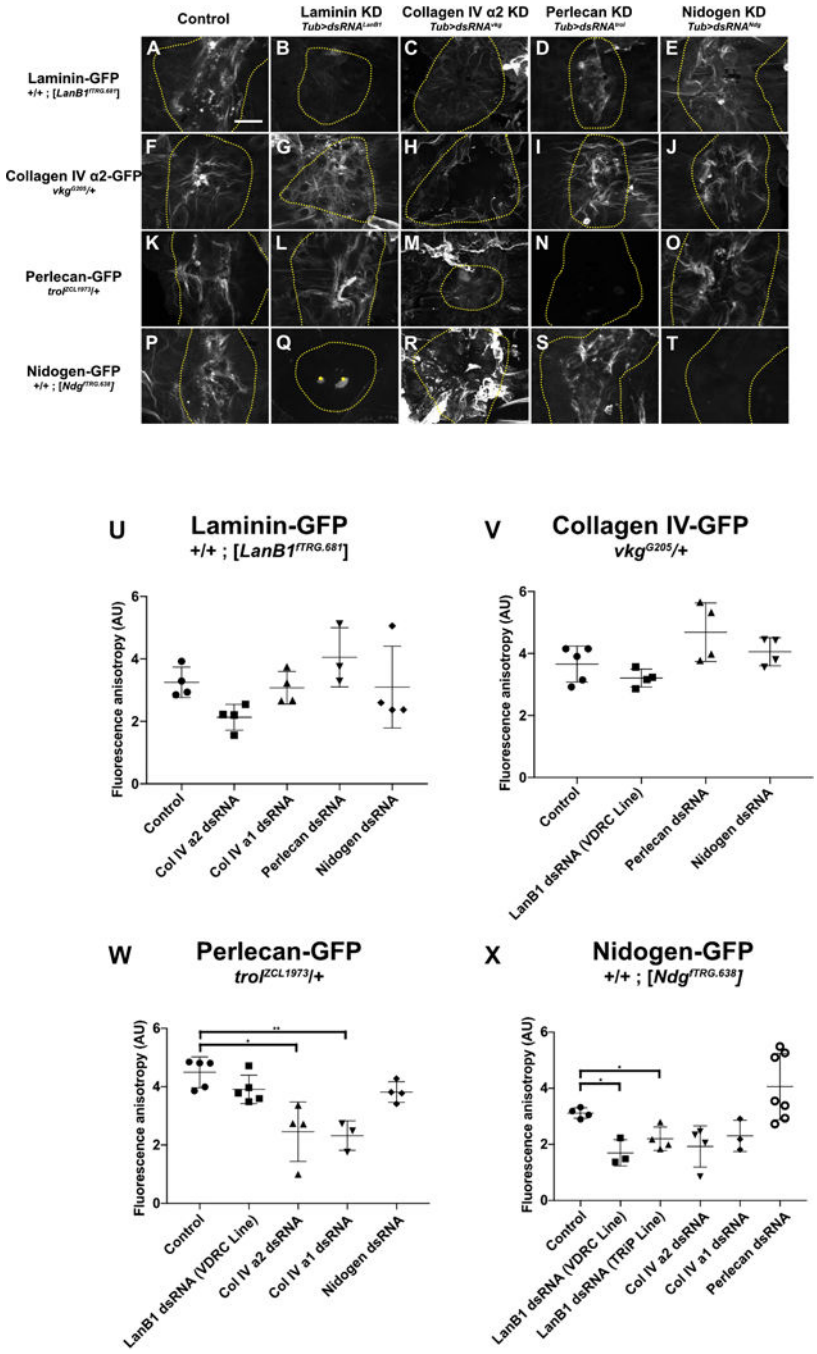

Figure 6: Hierarchy of basement membrane assembly during repair.

A-E) Laminin assembled into repaired basement membrane independent of any other basement membrane proteins. **F-J)** Collagen IV assembled into repaired basement membrane independent of any other basement membrane proteins. **K-O)** Although perlecan assembled into repaired basement membrane independent of any other basement membrane proteins, its assembly into the scar required collagen IV **(M)**. **P-T)** Nidogen required laminin **(Q)** but not collagen IV **(R)** or perlecan **(S)** to assemble into repaired basement membrane. In collagen knock-down wounds **(C,H,M,R)**, scars appear to extend outside the wound area,

see text. In panel **Q**, the bright dots at the wound center (marked by yellow stars) are autofluorescent melanization, see Experimental Procedures. **U-X)** Quantification of fluorescence anisotropy in repaired basement membranes. * indicates $p \leq 0.05$, ** indicates $p \leq 0.01$. Unless otherwise indicated, no significant difference was observed. Scale bar, 50 μm.

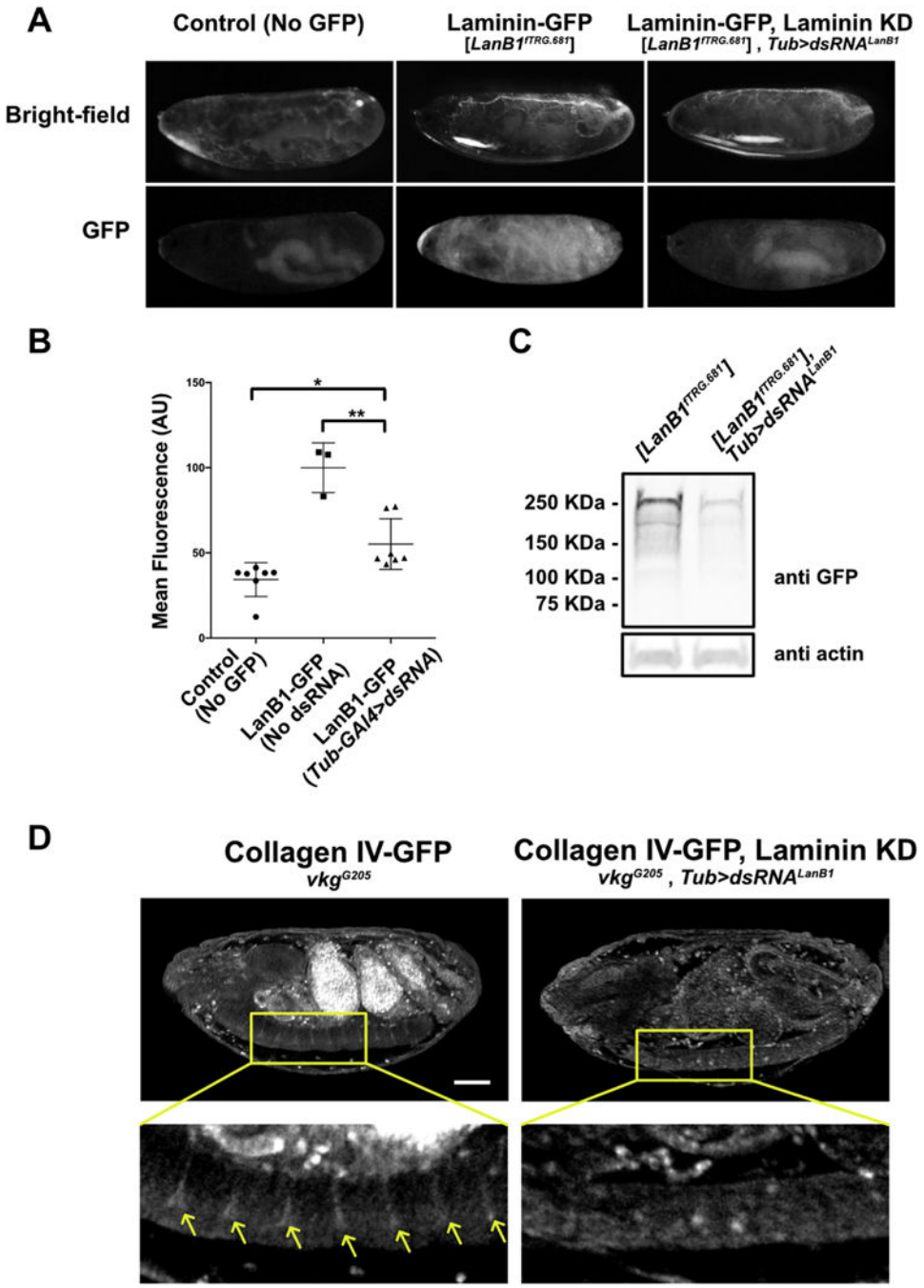

Figure 7: The requirement for laminin is different between basement membrane *de novo* assembly and repair.

A) Expression of dsRNA against *LanB1* knocked down LanB1-GFP levels in stage 16– 17 embryos, as determined by GFP fluorescence. **B)** Quantification of GFP fluorescence in embryos showed dsRNA against *LanB1* reduced LanB1-GFP levels by 68%. **C)** For comparison, expression of the same dsRNA against *LanB1* in larvae depleted LanB1-GFP by 71% as measured by western blot (see also Fig. S3). **D)** Expression of dsRNA against *LanB1* was sufficient to disrupt collagen IV deposition into the basement membrane of

ventral nerve cord channels in stage 16–17 embryos, as visible in controls (yellow arrows) ($N \geq 3$). Scale bar, 50 μm.

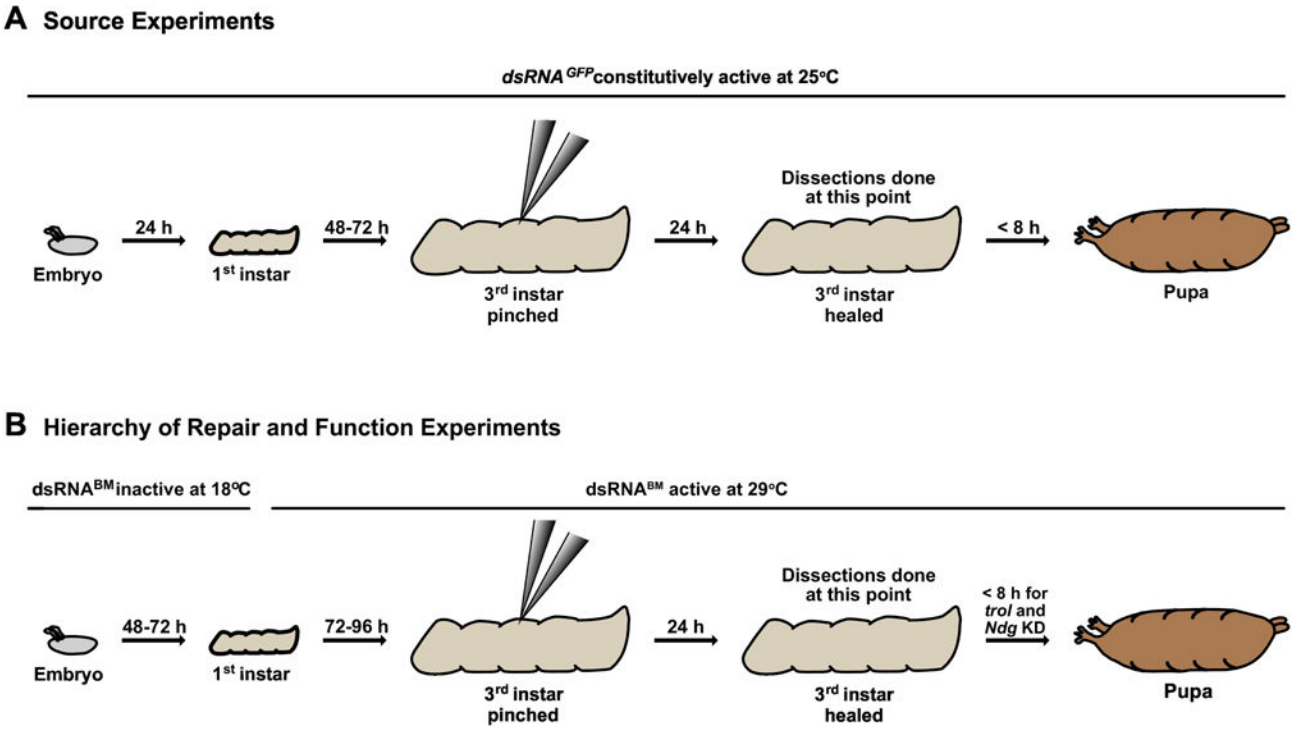

Figure 8: Timeline of experimental protocols for gene knockdown, showing larval development, dsRNA expression, and wounding.

A) For all basement membrane source experiments, animals were maintained at 25°C. Larvae developed to early 3rd instars, were pinched, and usually recovered 24 h before dissecting. For experiments where no wound was inflicted, larvae developed to late 3rd instar prior to dissecting. **B)** For basement membrane hierarchy of repair and function experiments in which *LanB1, vkg*, or *trol* was knocked down, embryos were laid and allowed to develop to 1st instar larvae at 18°C, with dsRNA not expressed. During 1st instar, bottles were shifted to 29°C to promote dsRNA expression, and larvae developed to early 3rd instar prior to wounding. After wounding, larvae recovered for 24 h at 29°C prior to dissecting. For *Ndg* KD experiments, bottles were maintained at 29°C for the entire experiment (not shown). Only control, *trol* KD and *Ndg* KD larvae were capable of pupariating. $dsRNA^{BM}$ denotes dsRNA against *vkg, trol,* or *LanB1.*

Table 1:

Fly Stocks

Genotype	Source
LanB1GFP	VDRC 318180
vkgGFP^{791}	Sally Horne-Badovinac, U. Chicago [44]
vkgGFP^{205}	[45]
trolGFP^{1973}	[45]
NdgGFP	VDRC 318629
w^{1118}	Todd Laverty, Janelia Farm
UAS-GFP^{S65T}	BDSC 1522
Tub-Gal4/TM6B	[46]
e22c-Gal4	BDSC 5083
A58-Gal4/TM6B	Michael Galko, MD Anderson Cancer Center
Pnr-Gal4/TM6B	Beth Stronach, University of Pittsburgh
Hml-Gal4	BDSC 30139
Mhc-Gal4	BDSC 55133
C564-Gal4	Kathryn V. Anderson, Sloan Kettering
UAS-dsRNA^{GFP}	BDSC 9330
UAS-dsRNA^{vkg}	VDRC 106812
UAS-dsRNA^{Col4A1}	BDSC 44520
w; UAS-dsRNA^{LanB1}	VDRC 23121 (main line used)
y sc v; UAS-dsRNA^{LanB1}	BDSC 42616 (alternate line)
UAS-dsRN^{trol}	VDRC 1110494
UAS-dsRNA^{Ndg}	VDRC 109625
w; VkgGFP^{205}; TubGal4, TubGal80^{ts}/ SM6-TM6B	This study
w; VkgGFP^{791}; UAS-dsRNA^{GFP}	This study
w; UAS-dsRNA^{GFP}; LanB1GFP	This study
w; LanB1GFP TubGal4 TubGal80^{ts} / TM6B	This study
w TrolGFP^{1973}; UAS-dsRNA^{GFP}	This study
w TrolGFP^{1973}; TubGal4, TubGal80^{ts} / TM6B	This study
NdgGFP, UAS-dsRNA^{GFP}	This study
NdgGFP TubGal4 TubGal80^{ts} / TM6B	This study
w; vkgGFP^{205} / CyO, sChFP; TubGal4, TubGal80^{ts} / TM3, sChFP	This study
w; LanB1GFP TubGal4 TubGal80^{ts} / TM3, sChFP	This study
CyO, sChFP	BDSC 35523
TM3, sChFP	BDSC 35524